Journal of Electroanalytical Chemistry 642 (2010) 135–142

Contents lists available at ScienceDirect

Journal of Electroanalytical Chemistry

journal homepage: www.elsevier.com/locate/jelechem

$Ru(DMSO)_4Cl_2$ nano-aggregated Nafion membrane modified electrode for simultaneous electrochemical detection of hypoxanthine, xanthine and uric acid

Annamalai Senthil Kumar *, Puchakayala Swetha

Environmental and Analytical Chemistry Division, Department of Chemistry, School of Advanced Sciences, Vellore Institute of Technology University, Vellore 632 014, India

ARTICLE INFO

Article history:
Received 7 January 2010
Received in revised form 23 February 2010
Accepted 24 February 2010
Available online 26 February 2010

Keywords:
Hypoxanthine
Xanthine
Uric acid
Simultaneous detection
$Ru(DMSO)_4Cl_2$
Nafion

ABSTRACT

$Ru(DMSO)_4Cl_2$ is a good precursor complex in synthetic inorganic chemistry and also considered to be an efficient anti-cancer drug. Here in, we are reporting ~80 nm nano-aggregates of $Ru(DMSO)_4Cl_2$ complex stabilized Nafion membrane modified glassy carbon electrode (GCE/Nf–{RuDMSO–Cl–H_2O}–MME) for simultaneous electro-catalytic oxidations and separation-less detection of purine bases; uric acid (UA), xanthine (X) and hypoxanthine (Hx) in a physiological solution. The MME was characterized using solid state UV–Vis, X-ray photoelectron spectroscopy (XPS) and transmission electron-microscopy (TEM) techniques. It has been found that $Ru(DMSO)_4Cl_2$ undergoes dissolution reactions within the water rich hydrophilic micro-channels of Nafion membrane and get electro-statically stabilized as $[Ru^{II}Cl_x(DMSO)_y(H_2O)_{4-(x+y)}]^{n+}$ through the cationic sulphonic acid structures. The MME film behaves like metallic electronic conductor, investigated with $Fe(CN)_6^{3-/4-}$ redox couple. This new electrode shows efficient electrochemical sensing of the UA, X and Hx with a calibration windows (detection limit) up to 700 (0.372 μM), 500 (2.351 μM) and 300 μM (2.37 μM) respectively. The electrode shows exceptional stability and applicability to various real samples.

1. Introduction

Ruthenium dimethylsulphoxide-chloride complex, $Ru(DMSO)_4Cl_2$ is a well known precursor to prepare various Ru-complexes [1–5], which possess mutagenic properties and exhibits good anti-neoplastic activity against several murine metastatic tumor cells such as P388 leukemia, Lewis lung carcinoma, B16 melanoma and MCa mammary carcinoma [6–8]. The complex can cross over the cell membrane and interacts with DNA, especially guanine during the tumor deactivation [9]. Meanwhile, Nafion (Nf) membrane is a cationic exchanging polyperfluoro polymer of perfluroethylene backbone chains (hydrophobic nature) interconnected with reverse micellar type pendant sulphonic acid groups of channel diameter size ~4 nm (hydrophilic and anionic character) [10]. Nafion membranes have been used often in fuel cell applications and other areas including chemical and biochemical sensors and synthetic organic chemistry [10,11]. In further, Nafion membrane has also been utilized as a template to prepare nano-scale particulates inside its fine micro-channel networks [12–17]. First time in this work, we are reporting ~80 nm nano-aggregates of $Ru(DMSO)_4Cl_2$ complex stabilized Nafion colloidal solution (designated as Nf–{RuDMSO–Cl–H_2O}) and further as a molecular membrane film on a glassy carbon chemically modified electrode (designated as GCE/Nf–{RuDMSO–Cl–H_2O}–MME) for simultaneous electro-catalytic oxidation and sensing of purine metabolites, hypoxanthine (Hx), xanthine (X) and uric acid (UA) in a physiological pH. To the best of our knowledge $Ru(DMSO)_4Cl_2$ has never been used in any chemically modified electrode system so for.

Purine bases are found high concentration in meat and meat products, especially in the internal organs such as liver and kidney [18,19]. Purine metabolites pathway involves transformation of hypoxanthine → xanthine, xanthine → uric acid and uric acid → oxidized products. *Xanthine oxidase*, XOD is the specific enzyme that oxidizes Hx → X and X → UA, is present in the liver of human [20–23]. Abnormalities of the metabolites concentrations are sensitive indicators of certain pathologic states, including gout, xanthinuria, hyperuricemia, renal failure, toxaemia during pregnancy, etc. [22–24]. Since Hx and X are the precursors of UA and important intermediates in purine biosynthesis, simultaneous detection of these two compounds have become vital in food, biochemical and clinical diagnosis.

In order to simultaneously detect the Hx, X and UA, separation techniques based on HPLC [25,26] and capillary electrophoresis [27,28] coupled with photo-diode array spectrophotometer at UV wavelength in between 245 and 265 nm were often reported.

* Corresponding author. Tel.: +91 416 2202754.
E-mail address: askumarchem@yahoo.com (A.S. Kumar).

1572-6657/$ - see front matter © 2010 Elsevier B.V. All rights reserved.
doi:10.1016/j.jelechem.2010.02.031

Meanwhile, for the above purpose, electrochemical biosensors utilizing a chemically modified electrode (CME) composed of XOD enzyme/redox mediator systems were also investigated [29–31]. In general, these methods are complicated, time consuming and several difficulties have been found to achieve satisfactory separation, sensitivity and enzyme stability. In this regard, few non-enzyme based electrochemical methods for the simultaneous detection of Hx, X and UA were reported till date, with examples being, unmodified glassy carbon electrode in 1 M H_2SO_4 [32], carbon paste electrodes polarized in a dilute alkaline medium (2 mM NaOH + 10 mM $NaClO_4$) [33], pre-anodized (2 V vs. Ag/AgCl) Nontronite clay coated screen-printed electrode in pH 7.5 phosphate buffer solution (PBS) [34], grinded carbon electrode in pH 4.8 acetate buffer solution [35] and Nafion/lead–ruthenate pyrochlore chemically modified electrode (preliminary results) [36]. Unfortunately, existing electrodes were having complicated preparations along with series of surface activation and pre-concentration steps. Present method allows easy electrode preparation and simple detection procedure. The nano-aggregates of $Ru(DMSO)_4Cl_2$ complex stabilized Nf membrane may also offer a model to study the binding nature of biochemical's on the active complex site.

2. Experimental

2.1. Chemicals and reagents

The ruthenium complex, $Ru(DMSO)_4Cl_2$ (*recemic mixture of cis and trans*) was synthesized according to the published procedure and recrystallized in DMSO [37]. Nafion® 117 perflourinated ion-exchange powder, 5% weight solution in a mixture of lower aliphatic alcohols was obtained from Wago Chemical, Japan. The following chemicals were of analytical grade and were purchased from Sigma and Aldrich, India used as received without any further purification; uric acid, xanthine, hypoxanthine. Aqueous solutions were prepared using deionized and alkaline $KMnO_4$ distilled water (designated as DD water). Unless otherwise stated, pH 7 phosphate buffer solution (PBS) of I = 0.1 M was used as supporting electrolyte in this study.

2.2. Apparatus

Voltammetric measurements were carried out using CHI model 660C electrochemical work station, USA with 10 mL working volume. The three electrode system consists of glassy carbon (GCE) of 0.0707 cm^2 geometrical surface area and its chemically modified electrode (CME) as working electrode, Ag/AgCl with 3 M KCl as a reference electrode and platinum wire as counter electrode. The bio-analytical system (BAS, USA) polishing kit was used to polish the GCE surface. The surface of the GCE was cleaned both mechanically (polished with 1 μm alumina powder in the BAS polishing kit, cleaned with acetone and washed with DD water) and electrochemically (by performing cyclic voltammetry (CV) for 10 cycles in the potential window –0.4 V to 1.0 V vs. Ag/AgCl in pH 7 PBS solution). A 1 KW power, Model JY-2000 ICP optical emission spectrometer (Jobin Yvon, France) was used for the determination of Ru. Ruthenium concentration in the purified $Ru(DMSO)_4Cl_2$ sample is 650 μg/g. Surface morphology was determined by transmission electron-microscopy (TEM, JEOL-3010). X-ray photoelectron spectroscopic analysis (XPS, American Physical Electronics, PHI XI/ESCA PHI 1600) was done for ITO/Nf–{RuDMSO–Cl–H_2O}–MME with a binding energy resolution of 0.1 eV. Ex situ atomic force microscopic (AFM) analyses were carried out by using a CSPM4500 (China) instrument.

2.3. Procedures

Nf–{RuDMSO–Cl–H_2O} colloidal solution was first prepared by mixing 43 mg of $Ru(DMSO)_4Cl_2$ with 373 μL of 5% Nafion (Nf), followed by 10 min of sonication at room temperature ($T \sim 28$ °C). This procedure results in a clear orange–yellow colloidal solution (Nf–{RuDMSO–Cl–H_2O}) which is stable in the room temperature for 3 months. This solution served as a stock to further prepare membrane modified electrodes (MME). The GCE/Nf–{RuDMSO–Cl–H_2O}–MME was then prepared by following procedure: 2 μL of the Nf–{RuDMSO–Cl–H_2O} colloidal solution was drop coated on the cleaned GCE surface and allowed to dry for 20–30 min. The film was further electrochemically pretreated by continuous cycling (n = 20) in pH 7 PBS in the potential window –0.4 to 0.8 V vs. Ag/AgCl at scan rate (v) of 50 mV/s. There is no redox behavior observed for this system. Since dissolved oxygen do not influence the present electrochemical system, experiments were all performed with normal dissolved oxygen (DO). Differential pulse voltammetry (DPV) was used as a quantitative electrochemical tool for the simultaneous detection of the Hx, X and UA in a pH 7 PBS.

Two real samples, laboratory person (female) urine and commercial fresh chicken-flesh samples were taken for analysis. The urine sample was filtered and diluted to five times before routine analysis. The chicken-flesh sample of weight 2 mg was first homogenized with 10 mL of pH 7 PBS buffer and then filtered (dilution factor = 5). Aliquots (10 mL) were taken for the electroanalysis. Standard addition approach was adopted for the analysis of the above samples.

3. Results and discussion

3.1. Physico-chemical characterization

Fig. 1 shows typical solid state UV–Vis pattern of ITO/Nf–{RuDMSO–Cl–H_2O}–MME in comparison with solution phase spectra of $Ru(DMSO)_4Cl_2$ complex dissolved in a mixture of 80% ethanol and 20% DD water. In order to imitate the organic and aqueous behaviors of the Nafion, the above said solvent mixture was taken. The naked complex showed a λ_{max} at 360 nm (Fig. 1a), while the ITO/

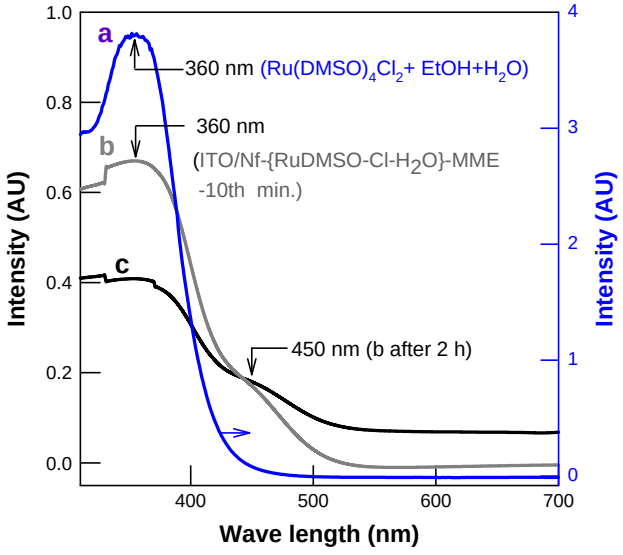

Fig. 1. Solution and solid state UV–Vis responses of 8.5 mg of $Ru(DMSO)_4Cl_2$ in 20% DD water + 80% ethanol mixture (without Nafion) (a) and ITO/Nf–{RuDMSO–Cl–H_2O}–MME at different time intervals (b and c).

Nf–{RuDMSO–Cl–H_2O}–MME resulted in a similar λ_{max} along with an additional shoulder like response at 450 nm (Fig. 1b). Change in the measurement time (10 min to 2 h) results to qualitatively similar UV–Vis patterns (Fig. 1c). The quantitative alterations might be due to change in the film thickness during the course of the drying time. Literature reports indicated that the $Ru(DMSO)_4Cl_2$ exhibits reversible *cis* and *trans* linkage isomerism, in which four S-bonded DMSO's were occupied in the square planner position of the octahedral configuration for the *trans* form [8,9,38]. On the other hand, three out of four DMSO's are S-bonded to the Ru in a facial configuration, while the last one is O-bonded in the *cis* form [9,38]. In further, both the forms were reported to be involved in rapid dissolution reaction with water [38] (Scheme 1). For instance, *cis*-$Ru(DMSO)_4Cl_2$ complex once dissolved in water, immediately releases the O-bonded DMSO and become *cis, fac*-[$Ru(DMSO)_3Cl_2(H_2O)$], which then under strong photo-irradiation (visible light; 400 nm) and thermal hydrolysis (~20 °C) leads to slow exchange of its Cl^- with H_2O to form $[Ru^{II}Cl_x(DMSO)_y(H_2O)_{4-(x+y)}]^{n+}$ complex as in the Scheme 1 [38]. This structural change could be identified from the UV–Vis spectroscopy, where a characteristic peak at 360 nm is observed for the *cis, fac*-[$Ru(DMSO)_3Cl_2(H_2O)$] [38]. Meanwhile, *trans* form of the respective complex resulted in the rapid formation to *trans, cis, cis*-$Ru(DMSO)_2Cl_2(H_2O)_2$ complex in water (λ_{max} ~ 300 nm) and finally to $[Ru^{II}Cl_x(DMSO)_y(H_2O)_{4-(x+y)}]^{n+}$ [9,38]. Note that both the *cis* and *trans* forms of the complexes yielded similar kinds of end product. Hence, the possible ruthenium complex species present in the ethanol + H_2O system is of *cis, fac*-[$Ru(DMSO)_3Cl_2(H_2O)$], while the complex encapsulated Nafion membrane might be of $[Ru^{II}Cl_x(DMSO)_y(H_2O)_{4-(x+y)}]^{n+}$/Nafion–$SO_3^-$ (Schemes 1 and 2).

Exact detail for the isomeric conversion within the film is unknown to us now. It is expected that the high concentration of sulphonic acid group ($-SO_3^- \cdot H^+$) present within the hydrophilic aquatic micro-channel structure of Nafion, might assist the *cis, fac*-[$Ru(DMSO)_3Cl_2(H_2O)$] → $[Ru^{II}Cl_x(DMSO)_y(H_2O)_{4-(x+y)}]^{n+}$ reaction in room temperature, which is then electro-statically stabilized within its anionic micro-channel structure of the Nafion (Scheme 2).

Nano-aggregates of the Ru-complex of average size 80 nm were seen as dark spots in Fig. 2, which is relatively higher than the expected micro-channel structure of the unmodified Nafion, ~4 nm. This may be due to the strong aggregation (as polynuclear Ru-complex)-induced expansion of the Nafion membrane pores, similar to the nano-aggregates of Mn_3O_4 within the Nafion [17]. Since the Nafion stabilized Ru-complex containing water and chloride as molecular ligands, it should be involved in inter multi-hydrogen bonding to form larger sized nano-aggregates as macro molecular architectures [39,40]. Hence, the size of Ru-complex formed within the Nafion's micro-channels appears to be controlled by the size of the reverse-micellar like ionic cluster structure of the membrane.

The XPS survey spectrum of the ITO/Nf–{RuDMSO–Cl–H_2O}–MME shows peaks related to Ru, S, Cl and O 1s species (Fig. 3). Ru 3d core energy XPS of the sample yielded well-defined doublet peaks; Ru $3d_{5/2}$ and $3d_{3/2}$, where BE of Ru is $3d_{5/2}$ = 285.4 eV, which is closer to a value of 285 eV for the Ru(II) oxidation state of ITO/Nafion–$Ru^{II}(bpy)_3^{2+}$ complex [41]. XPS of S 2p energy level shows existence of three different species; bonded DMSO (CH_3–**S**O–CH_3, 166.5 eV, bold letter denotes the active atom), free sulphonic acid; $-SO_3^-$ (167.6 eV) and un-bonded DM**S**O (164.8 eV, due to dissolution of one of the DMSO from the $Ru(DMSO)_4Cl_2$ core) are in analogues to related species at 166.3, 168.9 and 164.2 eV for the naked $Ru(DMSO)_4Cl_2$ and Ru–S containing heterocyclic complexes in the literature [42]. The Cl 2p energy level of the film shows couple of peaks at the BE values of 199 and 201.8 eV, which are relatively higher than the expected values of ~197.6 eV for the naked $Ru(DMSO)_4$**Cl**$_2$ [42]. Possibly involvement of strong H-bonding effect through –**Cl**–H–O–H– links within the Nafion membrane might be a reason to the BE shift in the higher energy side. The additional Cl 2p peak at 201.8 eV may be due to unknown impurity, which might be released from the $Ru(DMSO)_4Cl_2$ dissolution steps within the membrane. High resolution XPS of the O 1s attributed to existence of five different species; Ru–DMS**O** (531.6 eV), free $-SO_3^-$ (532.2 eV), un-bonded H_2**O** (533.8 eV), Ru–H_2**O** (534.6 eV) and –C–**O**–C linkages (536.6 eV) in comparison with the literature reports for the naked $Ru(DMSO)_4Cl_2$ (532 eV) [42], Nafion–$SO_3^- \cdot H^+$ (~332.5 eV) [41], H_2**O** adsorbed metal oxides (534 eV) [43], aqua–metal complex (534.1 eV) [44] and Nafion's ether link (~536 eV) [41] respectively. Collective information of the observation further supports the $[Ru^{II}Cl_x(DMSO)_y(H_2O)_{4-(x+y)}]^{n+}$ complex stabilized by anionic reverse-micellar like sulphonic sites structure of the Nafion.

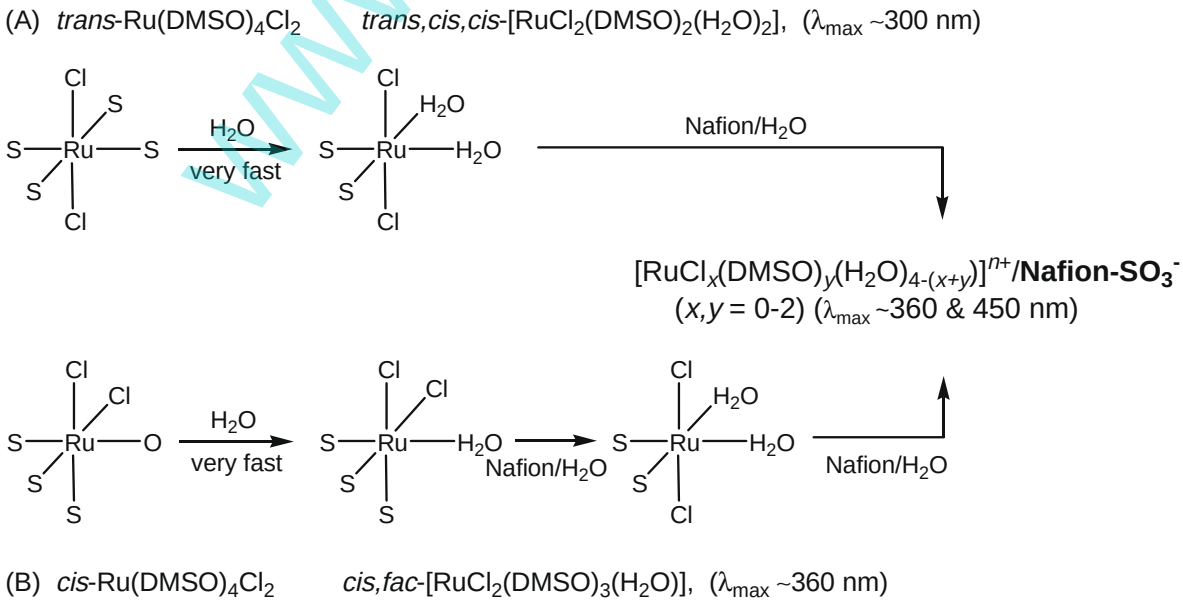

Scheme 1. Possible transformations of $Ru(DMSO)_4Cl_2$ isomers in presence of aqueous and Nafion systems. S = sulphur atom of the DMSO; O = oxygen atom of the DMSO.

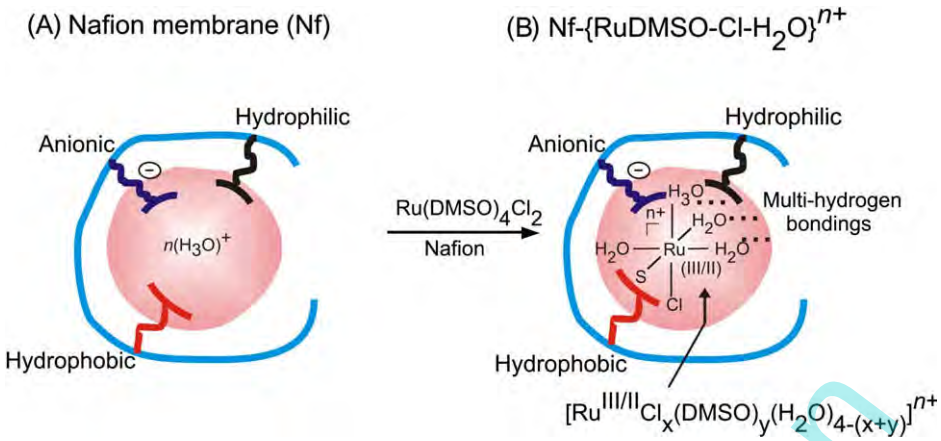

Scheme 2. Cartoon for the illustration of $[RuCl_x(DMSO)_y(H_2O)_{4-(x+y)}]^{n+}$ stabilized Nafion membrane system (i.e., Nf–{RuDMSO–Cl–H_2O}).

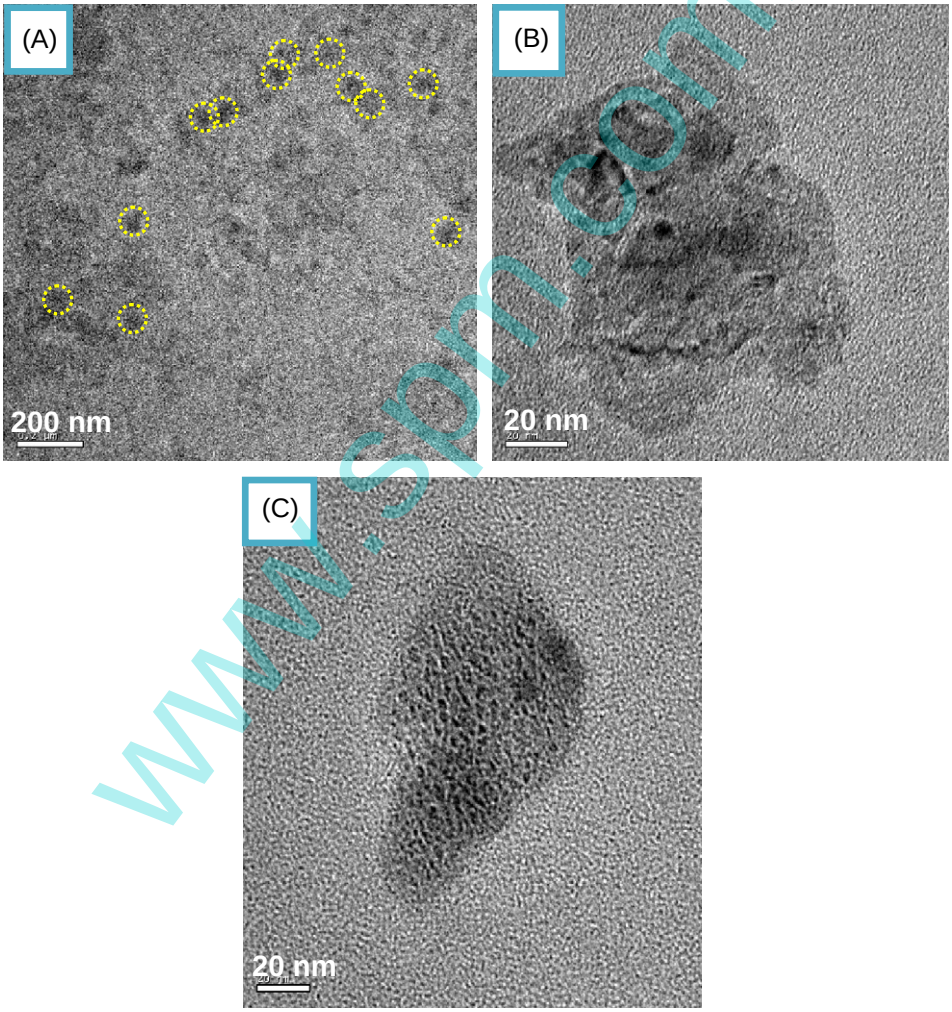

Fig. 2. TEM pictures of Nf–{RuDMSO–Cl–H_2O} system at different magnifications. Circled portions are representative nanoaggregate of the {RuDMSO–Cl–H_2O} species.

AFM image of the ITO modified Nf shows almost flatter topological structure, while Nafion modified Ru-complex shows nano-porous and contour structures of the underlying surface (Fig. S1), which is in parallel to the TEM observation and to the proposed nano-aggregated structures.

3.2. Electronic characteristic

Fig. 4 is the CV responses of $Fe(CN)_6^{3-}$ at MME, GCE/Nf and GCE. Since the Nafion membrane has anionic character, it is expected that the solution phase anionic $Fe(CN)_6^{3-}$ complex would strongly

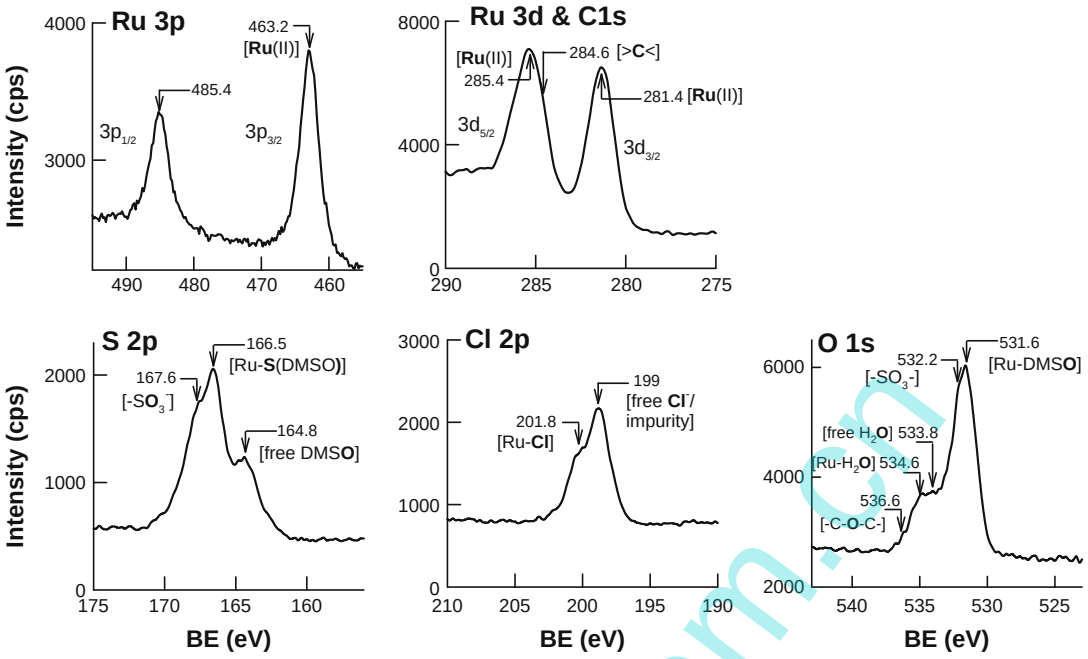

Fig. 3. High resolution XPS patterns of ITO/Nf–{RuDMSO–Cl–H_2O}–MME for Ru 3p, Ru 3d, S 2p, Cl 2p and O 1s atomic energy levels.

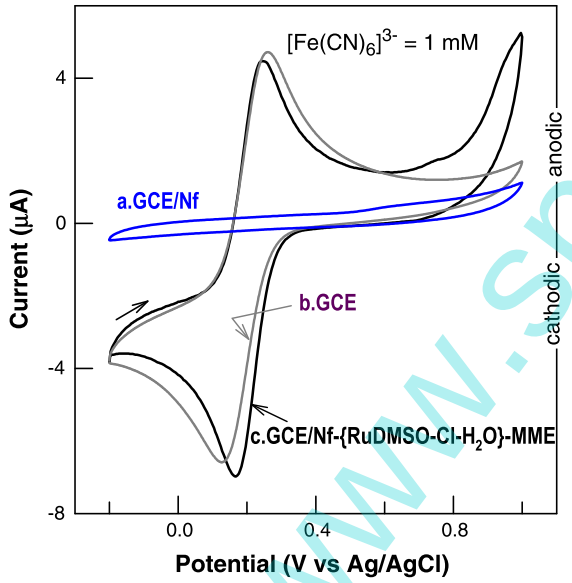

Fig. 4. CV response of various electrodes with 1 mM $K_3[Fe(CN)_6]$ in a pH 7 PBS at a v = 10 mV/s.

repelled from the MME's and GCE/Nf's outer surface, and hence absence of any characteristic redox feature. Unlike to the expectation, the bench-mark redox system showed a well-defined redox feature with an anodic (E_{pa}) and cathodic (E_{pc}) peak potentials of 240 and 170 mV vs. Ag/AgCl respectively in the MME. Calculated peak-to-peak separation value (ΔE_p) is 70 mV, which is closer to the ideal value of 60 mV. Meanwhile, under identical experimental condition, unmodified GCE showed ~2 times higher in the ΔE_p value (135 mV) and GCE/Nf failed to show any such response. The higher ΔE_p value with the GCE may be due to sluggish electron-transfer (ET) in neutral solution [45]. These observations implies that the $Ru(DMSO)_4Cl_2$ incorporated Nafion membrane behave as a perfect metal like electronic conductor with improved ET behavior. It is expected that Nafion's free sulphonic acid groups, $-SO_3^-$ were all neutralized and masked by the $[Ru^{II}Cl_x(DMSO)_y(H_2O)_{4-(x+y)}]^{n+}$ complex aggregates and there by behave as active site for the electronic conduction [11].

3.3. Electrochemical and catalytic behaviors

Curves named 'a' in Fig. 5 are typical CV and DPV responses of GCE/Nf–{RuDMSO–Cl–H_2O}–MME in blank electrolyte. No significant redox peak response was noticed, but their electrocatalytic activities towards purine bases are obvious. Fig. 5 shows comparative CV (A–C) and DPV (D–F) responses of GCE/Nf–{RuDMSO–Cl–H_2O}–MME (b), GCE (c) and GCE/Nf (d) discretely with uric acid (UA), hypoxanthine (Hx) and xanthine (X) in a pH 7 PBS. As can be seen from the CV of the uric acid, GCE shows a marked anodic peak at 0.3 V vs. Ag/AgCl, while the MME showed twice increase in the anodic current over the GCE with closer in the peak potential. For the case of xanthine oxidation by CV, the MME showed 200 mV reduction in the over-potential value (η, E_{pa} = 0.65 V vs. Ag/AgCl) and ~1.5 times increase in the peak current over the GCE/Nf. Similarly for hypoxanthine case, the MME yielded a defined oxidation peak at 1 V vs. Ag/AgCl, while the GCE and GCE/Nf failed to show any such defined oxidation peaks. Parallel DPV responses support the above observation (Fig. 5D–F). These observations attribute to electro-catalytic features of the MME towards the purine bases in this work (relatively weak electro-catalytic effect to uric acid). Observation of negative potential shift in the DPV for the UA oxidation on the MME with respect to the GCE (Fig. 5D), unlike to the same oxidation potential by CV in Fig. 5A, may be due to applied amplitude and pulse effects, which may leads to some temporary surface interaction of UA on the MME. This is infact advantage of using the DPV as qualitative tool in this work.

Effect of scan rate (v) on the CV oxidation of the analytes at the MME shows systematic increase in the peak current responses (Fig. S2A–C). Double logarithmic plot of log (i_{pa}) vs. log (v) yielded linear line with a slope ($\partial \log i_{pa}/\partial \log v$) values of 0.4, 0.4 and 0.43 respectively for the UA, X and Hx, which is closer to a value of 0.5 (Fig. S2D), which indicates the mechanism based on diffusion-controlled reaction pathways. There is no sign of the analyte's peaks in

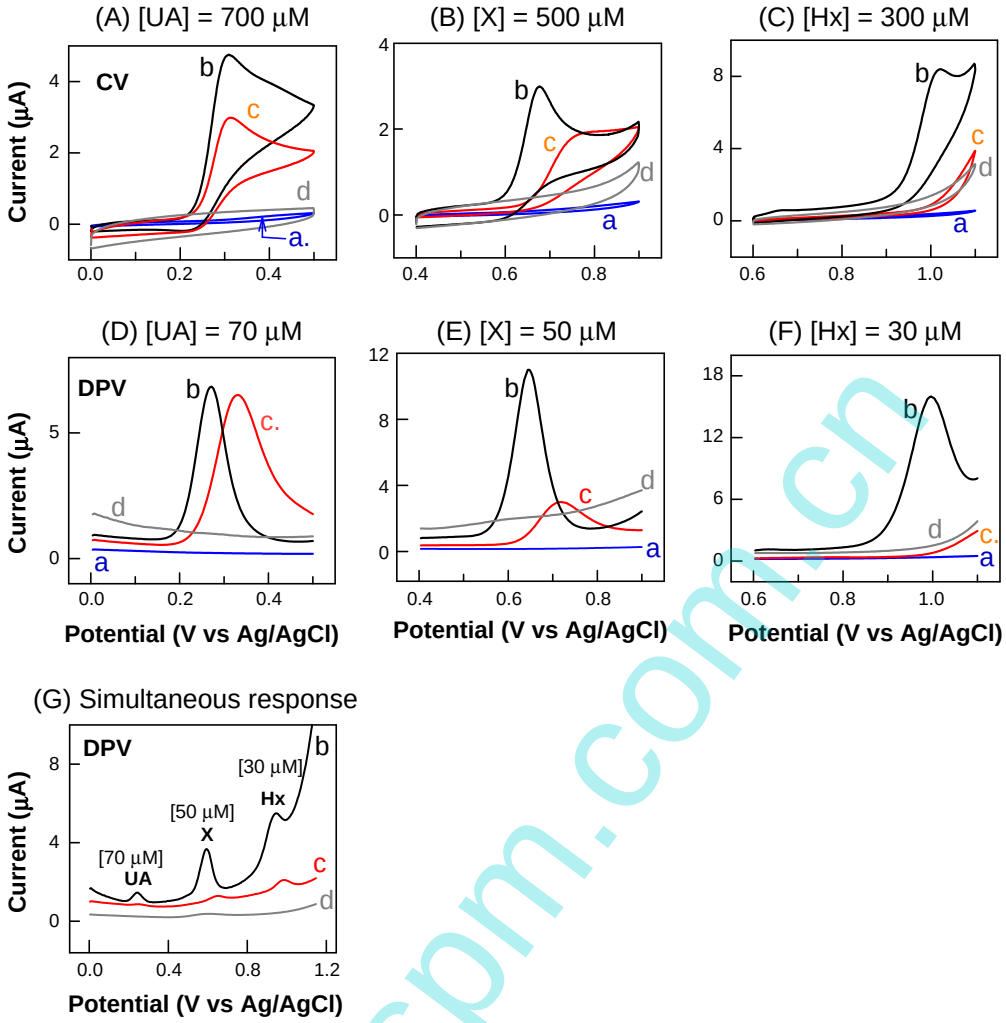

Fig. 5. Comparative CV (A–C) and DPV (D–F) responses of various purine bases at GCE/Nf–{RuDMSO–Cl–H_2O}–MME (b), GCE (c) and GCE/Nf (d) in a pH 7 PBS. Curve (a) is response of the MME with absence of analyte. (G) Typical DPV simultaneous response. CV scan rate (v) = 10 mV/s. For DPV analysis: amplitude = 50 mV; increment potential = 4 mV; pulse width = 60 ms; sampling width = 20 ms and pulse period = 200 s.

a medium transferred blank solution by CV, unlike to the previous pre-anodized Nontronite clay modified electrodes with strong adsorption effect [34]. This is a clear advantage to easy renewal of the working surface. Tafel slope values ($\partial \log E_{pa}/\partial \log v$) were indirectly constructed from the E_{pa} vs. log (v) plot, and the values are 78, 78 and 48 respectively for the UA, X and Hx (Table 1). Corresponding anodic transfer coefficient, α_a values were 0.4, 0.4 and 0.61, which indicates symmetry in the energy barrier for the electron-transfer reactions.

Typical DPV responses for the simultaneous detection of the purine bases on various electrodes were given in Fig. 5G. GCE/Nf–{RuDMSO–Cl–H_2O}–MME yielded well-defined, well separated and ~10 times increase in the peaks current signals at 0.24, 0.590 and 0.90 V vs. Ag/AgCl respectively over the unmodified electrodes with 50–150 mV reduction in the over-potential (η) values, due to the electrocatalytic function of the underlying MME electrode (UA shows relatively lower electro-catalytic effect). Fig. S3 shows effect of solution pH on the simultaneous oxidations of the three analytes by DPV in the window pH 3–8. The UA's peak current response attained a maxima value at pH 6–7, before and after the optimal value ~2 times lowered current signals were observed. This trend is almost same to X and Hx cases also. Exact details for the behavioral changes are unknown for us now. Since pH 7 PBS showed relatively higher current signals to all the three analytes, this pH was chosen as optimal for further analysis.

Effect of UA, X and Hx concentration (calibration) on the simultaneous detection of the individual analyte was next studied by systematically increasing one analyte concentration with other two fixed as in the Fig. 6. The DPV of the UA shows regular increase in the UA current signals up to 700 μM. Constructed calibration plot was linear in that window with a slope and regression (R) coefficient values of 1.84×10^{-2} μA/μM and 0.9985 respectively. Ten repeated DPV measurements (n = 10) of 20 μM UA resulted to a relative standard deviation (RSD) value of 3.59% (Fig. S4). Calculated detection limit, D_L (signal-to-noise ratio, S/N = 3) value was

Table 1
Kinetic parameters for the electro-catalytic oxidation of purine bases on GCE/Nf–{RuDMSO–Cl–H_2O}–MME.

Parameters	Uric acid	Xanthine	Hypoxanthine
Potential (V vs. Ag/AgCl)	0–0.5 V	0.4–0.9 V	0.6–1.1 V
Surface coverage, Γ_{Ru} ($\times$10–12 mol cm^{-2})	0.0113	0.213	0.793
K_M (mmol dm^{-3})	12.29	1.196	0.256
k'_e (cm s^{-1})	0.003	0.008	0.0159
k_c (s^{-1})	3.1×10^6	4.5×10^4	1.9×10^4
Tafel slope (mV/decade)	78	78	48
Transfer coefficient, α	0.40	0.40	0.61

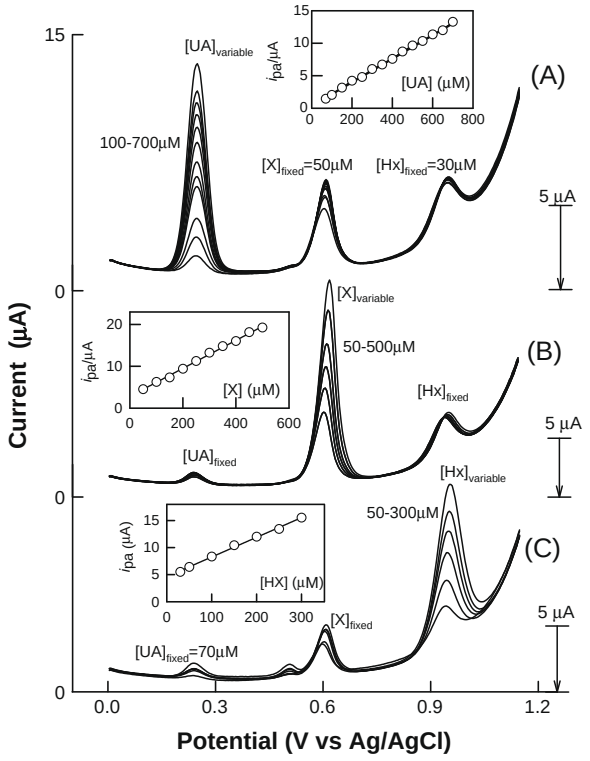

Fig. 6. Typical DPV responses for the simultaneous detection of uric acid, xanthine and hypoxanthine with respect to one another using GCE/Nf–{RuDMSO–Cl–H_2O}–MME in a pH 7 PBS. Plot of i_{pa} vs. analyte concentration, [analyte] were given as respective insert figures.

0.372 μM. Similarly the slope (R), RSD and D_L values for X and Hx are: 3.37×10^{-2} μA/μM ($R = 0.9972$), 3.53% ([X] = 20 μM, $n = 10$) and 2.351 μM and 3.64×10^{-2} μA/μM ($R = 0.9969$), 5% ([Hx] = 20 μM, $n = 10$) and 2.37 μM respectively on the GCE/Nf–{RuDMSO–Cl–H_2O}–MME in a pH 7 PBS. Appreciable RSD values with the MME indicate good reproducibility of the working electrode towards the purine analysis, without any surface fouling or poisoning effects in this work. Obtained D_L values were comparable with that of the 2 V vs. Ag/AgCl pre-anodized and 60 s pre-concentrated Nontronite modified electrodes in neutral buffer solution [34], yet without pre-anodization and pre-concentration procedures. Note that fraction of the analytes get oxidized (Hx → X and X → UA) on the working electrode interphase during the anodic sweep, which may further result in slight variation in the current signal of the fixed analytes [35].

Surface concentration of electro-active ruthenium species (Γ_{Ru}) were estimated by performing chrono-coulometric experiment in the respective analyte working potential windows and the values are; 0.0113 (0–0.5 V), 0.213 (0.4–0.9 V) and 0.793×10^{-12} mol cm^{-2} (0.6–1.1 V vs. Ag/AgCl) (Fig. S3 and Table 1). Reaction order, [$\partial \log (i_{pa}/\mu A)/\partial \log$ (analyte/μM)] was calculated from the plot of log (i_{pa}) vs. log (analyte) and the values are ~1 for UA and X, and 0.5 for Hx on the GCE/Nf–{RuDMSO–Cl–H_2O}–MME (figures were not included). The lower the reaction order with Hx may be due to the interference of oxygen evolution reaction at the high operating potentials. Concern about the electro-catalytic mechanism, we propose a kinetics based on Michaelis–Menten (MM) type of enzyme-analyte mechanism as per our previous thin film electrocatalytic system with monolayer surface active site concentration [11,36]. In that mechanism, first the catalyst/analyte form an intermediate complex (Step-1) and then decompose to product with reduced form of the catalytic active site (Step-2), this in turn results back to the active form by electrochemical oxidation (Step-3) as in Scheme 3 for an example of xanthine oxidation. Calibration plots obtained in Fig. 6 were further taken for calculation of respective kinetic parameters, K_m = Michaelis–Menten rate constant, k_c = catalytic rate constant and k'_e = heterogeneous electrochemical rate constant using Lineweaver–Burke (LB) plot method (Fig. S5 and Table 1) from the following simplified linear equation [36].

$$1/i_{pa} = K_m/nFAk_c\Gamma_{Ru}[\text{purine}] + 1/nFAk_c\Gamma_{Ru} = S_{LB}[\text{purine}] + I_{LB} \quad (1)$$

$$S_{LB} = K_m/nFAk_c\Gamma_{Ru}[\text{purine}] \text{ and } I_{LB} = 1/nFAk_c\Gamma_{Ru} \quad (2)$$

In the above equation S and I denote the slope and intercept value of the linearized equation, respectively and other symbols having its usual significance. The heterogeneous rate constant, k'_e value was calculated by substituting the k_c, Γ_{Ru} (Fig. S6) and K_m in the equation $k'_e = k_c\Gamma_{Ru}/K_m$, and the measured values were given in Table 1. Obtained k_c values in this work were ~3 order high over a bio-mimicking enzyme, based on Nafion/lead–ruthenium oxide pyrochlore chemically modified electrode towards various biomolecules including purine bases [11,36].

3.4. Analytical application

Practical application of the GCE/Nf–{RuDMSO–Cl–H_2O}–MME was further tested by measuring the concentration of uric acid and xanthine in human-urine and xanthine in chicken samples as in Fig. S7. DPV of the MME shows specific uric acid oxidation signal at 0.3 V (Fig. S7A) and xanthine signal at 0.70 V vs. Ag/AgCl (Fig. S7B) for the urine sample. Further spike of standard concentration of uric acid (50 μM) and xanthine (50 μM) to the urine sample, shows systematic increase in the peak current values on top of the respective oxidation potentials, which confirm the peaks due to uric acid and xanthine species in the urine real sample. Similarly, the xanthine in chicken shows an oxidation peak current signal at 0.70 V vs. Ag/AgCl and the signal get increases uniformly upon spiking of standard xanthine (Fig. S7C). The results obtained for

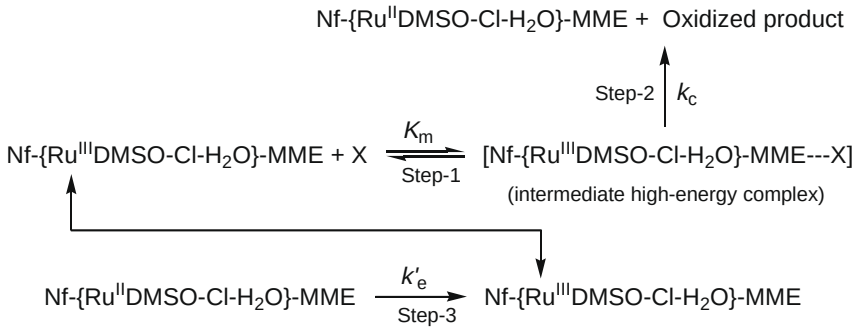

Scheme 3. Michaelis–Menten kinetic pathway for the electro-catalytic oxidation of xanthine (X) on GCE/Nf–{RuDMSO–Cl–H_2O}–MME.

Table 2
Real samples analysis of purine bases for urine and chicken samples using GCE/Nf–{RuDMSO–Cl–H_2O}–MME.

Parameters	Urine		Chicken
	Uric acid	Xanthine	Xanthine
Linear equation	$y = 0.147x + 0.952$	$y = 0.0104x + 0.863$	$y = 0.011x + 0.153$
Regression	0.999	0.999	0.996
Detected/ original (μM)	14.93	8.56	1.81
Spike (μM)	50	50	50
After spike (μM)	47.55	50.67	49.45
Recovery (%)	95.10	101.34	98.9

the two real samples were summarized in Table 2. Absence of uric acid peak with the chicken-flesh sample denotes the freshness of the sample. The better recovery values of the MME indicated that the MME could be efficiently used for the determination of purine bases in the various real samples. Finally investigated stability check for a period of a month time (Fig. S8), showed ~5% alteration in the i_{pa} with 50 mV positive E_{pa} shift, which further indicated that the working electrode is appreciably stable without any fouling effects.

4. Conclusions

$Ru(DMSO)_4Cl_2$ complex was used for the first time in the literature as mediator to prepare a new chemically modified electrode with Nafion (GCE/Nf–{RuDMSO–Cl–H_2O}–MME) and further to simultaneous electrochemical detection of purine bases; uric acid, xanthine and hypoxanthine utilizing the electro-catalytic effect in a physiological solution. Physico-chemical characterization by solid state UV–Vis, TEM and XPS have suggested that the $Ru(DMSO)_4Cl_2$ get converted to ~80 nm aggregates of cationic $[Ru^{II}Cl_x(DMSO)_y(H_2O)_{4-(x+y)}]^{n+}$ particles, which then stabilized within the water and sulphonic acid rich micro-channel structure of the Nafion membrane. The new membrane modified electrode (MME) showed unusual metal like electronic conductivity, which was investigated through $Fe(CN)_6^{3-/4-}$ redox couple, showed a superior response to the classical GCE electrode. Possible mechanism was proposed in terms of Michaelis–Menten type of enzyme-analyte reaction kinetics with the MME. Two real sample analyses were successfully demonstrated with appreciable recoveries. Important advantage of the present analytical approach is, the working MME can be prepared on any conducting substrates unlike to the literature reports, for example, on the disposable type screen-printed electrodes and ITO without any activation procedures and further to the purine bases analysis in a physiological pH.

Acknowledgments

The Authors gratefully acknowledge financial support from the Department of Science and Technology (DST), India. We thank Prof. Jyh-Myng Zen and Dr. Jen-Lin Chang for AFM and XPS analyses. We also thank material science division, IIT Madras for the TEM characterization.

Appendix A. Supplementary material

Supplementary data associated with this article can be found, in the online version, at doi:10.1016/j.jelechem.2010.02.031.

References

[1] T.J. Meyer, M.H.V. Huynh, Inorg. Chem. 42 (2003) 8140.
[2] J.-S. Huang, G.-A. Yu, J. Xie, K.-M. Wong, N. Zhu, C.-M. Che, Inorg. Chem. 47 (2008) 9166.
[3] H. Sarmistha, A. Rama, S.-M. Peng, G.-H. Lee, M.G.B. Drew, S. Bhattacharya, Inorg. Chem. 45 (2006) 9654.
[4] R. Zong, R.P. Thummel, J. Am. Chem. Soc. 127 (2005) 12802.
[5] J.J. Rack, H.B. Gray, Inorg. Chem. 38 (1999) 2.
[6] C. Monti-Bragadin, M. Giacca, L. Dolzani, M. Tamaro, Inorg. Chim. Acta 137 (1987) 31.
[7] G. Sava, S. Zorzet, T. Giraldi, G. Mestroni, G. Zassinovich, Eur. J. Cancer Clin. Oncol. 20 (1984) 841.
[8] I. Bratsos, A. Bergamo, G. Sava, T. Gianferrara, E. Zangrando, E. Alessio, J. Inorg. Biochem. 102 (2008) 606.
[9] E. Alessio, G. Mestroni, G. Nardin, W.M. Attia, M. Calligaris, G. Sava, S. Zorzet, Inorg. Chem. 27 (1988) 4099.
[10] K.A. Mauritz, R.B. Moore, Chem. Rev. 104 (2004) 4535.
[11] J.-M. Zen, A.S. Kumar, Acc. Chem. Res. 34 (2001) 772.
[12] P. Liu, J. Bandara, Y. Lin, D. Elgin, L.F. Allard, Y.-P. Sun, Langmuir 18 (2002) 10398.
[13] A.S. Kumar, T. Tanase, M. Iida, Langmuir 23 (2007) 391.
[14] J. Li, S. Zhang, P. Zhang, D. Liu, Z.-X. Guo, C. Ye, D. Zhu, Chem. Mater. 15 (2003) 4739.
[15] Z.-X. Guo, N. Sun, J. Li, L. Dai, D. Zhu, Langmuir 18 (2002) 9017.
[16] H.W. Rollins, F. Lin, J. Johnson, J.J. Ma, J.-T. Liu, M.-H. Tu, D.D. DesMarteau, Y.-P. Sun, Langmuir 16 (2000) 8031.
[17] M. Ludvigsson, J. Lindgren, J. Tegenfeld, J. Mater. Chem. 11 (2001) 1269.
[18] H. Rosemeyer, Chem. Biodivers. 1 (2004) 361.
[19] P. Badenoch-Jones, P.J. Buttery, Biochem. J. 158 (1976) 549.
[20] H. John, T. Ayvazian, S. Skupp, J. Clin. Invest. 44 (1965) 1248.
[21] T. Yamamoto, Y. Moriwaki, S. Takahashi, Clin. Chim. Acta 356 (2005) 35.
[22] E.S. West, W.R. Todd, Howard Mason, J.T.V. Bruggen, Text Book of Biochemistry, fourth ed., Oxoford & IBH Publishing Co., New Delhi, 1996.
[23] N.V. Bhagavan, Medical Biochemistry, fourth ed., Academic Press, USA, 2002.
[24] J.S.N. Dutt, M.F. Cardosi, J. Davis, Analyst 128 (2003) 811.
[25] S. Sumi, K. Kidouchi, S. Ohba, Y. Wada, J. Chromatogr. B 670 (1995) 376.
[26] K. Safranow, Z. Machoy, K. Ciechanowski, Anal. Biochem. 286 (2000) 224.
[27] Z.K. Shihabi, M.E. Hinsdale, A.J. Bleyer, J. Chromatogr. B 669 (1995) 163.
[28] T. Wessela, C. Lanversa, S. Fruendb, G. Hempel, J. Chromatogr. A 894 (2000) 157.
[29] G. Arai, S. Takahashi, I. Yasumori, J. Electroanal. Chem. 410 (1996) 173.
[30] L. Mao, F. Xu, Q. Xu, L. Jin, Anal. Biochem. 292 (2001) 94.
[31] M.-A. Carsol, G. Volpe, M. Mascini, Talanta 44 (1997) 2151.
[32] T. Yao, T. Wasa, S. Musha, Bull. Chem. Soc. Jpn. 50 (1977) 2917.
[33] X. Cai, K. Kalcher, C. Neuhold, Fresen. J. Anal. Chem. 348 (1994) 660.
[34] J.-M. Zen, Y.-Y. Lai, H.-H. Yang, A.S. Kumar, Sens. Actuators B 84 (2002) 237.
[35] S. Hason, S. Stepankova, A. Kourilova, V. Vetterl, J. Lata, M. Fojta, F. Jelen, Anal. Chem. 81 (2009) 4302.
[36] J.-M. Zen, Y.-Yen Lai, G. Ilangovan, A.S. Kumar, Electroanalysis 12 (2000) 280.
[37] I.P. Evans, A. Spencer, G.J. Wilkinson, J. Chem. Soc. Dalton Trans. (1973) 204.
[38] M. Brindell, G. Stochel, V. Bertolasi, R. Boaretto, S. Sostero, Eur. J. Inorg. Chem. (2007) 2353.
[39] X.-Yan Chen, P. Cheng, B. Zhao, S.-Ping Yan, D.-Zheng Liao, Z.-Hu Jiang, J. Mol. Struct. 655 (2003) 179.
[40] N. Metanis, A. Brik, P.E. Dawson, E. Keinan, J. Am. Chem. Soc. 126 (2004) 12726.
[41] D. Susac, M. Kono, K.C. Wong, K.A.R. Mitchell, Appl. Surf. Sci. 174 (2001) 43.
[42] P.L. Chanp, A.H. Chand, A. Frost, B. James, Can. J. Chem. 66 (1988) 117.
[43] M.A. Henderson, S.A. Chambers, Surf. Sci. 449 (2000) 135.
[44] A.S. Kumar, P.-Y. Chen, S.H. Chien, J.-M. Zen, Electroanalysis 17 (2005) 210.
[45] M.D. Rubianes, G.A. Rivas, Anal. Chim. Acta 440 (2001) 99.